

Measurement of inclusive differential cross sections for $\Upsilon(1S)$ production in $p\bar{p}$ collisions at $\sqrt{s} = 1.96$ TeV

V.M. Abazov,³⁵ B. Abbott,⁷² M. Abolins,⁶³ B.S. Acharya,²⁹ M. Adams,⁵⁰ T. Adams,⁴⁸ M. Agelou,¹⁸ J.-L. Agram,¹⁹ S.H. Ahn,³¹ M. Ahsan,⁵⁷ G.D. Alexeev,³⁵ G. Alkhazov,³⁹ A. Alton,⁶² G. Alverson,⁶¹ G.A. Alves,² M. Anastasoaie,³⁴ T. Andeen,⁵² S. Anderson,⁴⁴ B. Andrieu,¹⁷ Y. Arnoud,¹⁴ A. Askew,⁴⁸ B. Åsman,⁴⁰ A.C.S. Assis Jesus,³ O. Atramentov,⁵⁵ C. Autermann,²¹ C. Avila,⁸ F. Badaud,¹³ A. Baden,⁵⁹ B. Baldin,⁴⁹ P.W. Balm,³³ S. Banerjee,²⁹ E. Barberis,⁶¹ P. Bargassa,⁷⁶ P. Baringer,⁵⁶ C. Barnes,⁴² J. Barreto,² J.F. Bartlett,⁴⁹ U. Bassler,¹⁷ D. Bauer,⁵³ A. Bean,⁵⁶ S. Beauceron,¹⁷ M. Begel,⁶⁸ A. Bellavance,⁶⁵ S.B. Beri,²⁷ G. Bernardi,¹⁷ R. Bernhard,^{49,*} I. Bertram,⁴¹ M. Besançon,¹⁸ R. Beuselinck,⁴² V.A. Bezzubov,³⁸ P.C. Bhat,⁴⁹ V. Bhatnagar,²⁷ M. Binder,²⁵ C. Biscarat,⁴¹ K.M. Black,⁶⁰ I. Blackler,⁴² G. Blazey,⁵¹ F. Blekman,³³ S. Blessing,⁴⁸ D. Bloch,¹⁹ U. Blumenschein,²³ A. Boehnlein,⁴⁹ O. Boeriu,⁵⁴ T.A. Bolton,⁵⁷ F. Borcherding,⁴⁹ G. Borissov,⁴¹ K. Bos,³³ T. Bose,⁶⁷ A. Brandt,⁷⁴ R. Brock,⁶³ G. Brooijmans,⁶⁷ A. Bross,⁴⁹ N.J. Buchanan,⁴⁸ D. Buchholz,⁵² M. Buehler,⁵⁰ V. Buescher,²³ S. Burdin,⁴⁹ T.H. Burnett,⁷⁸ E. Busato,¹⁷ J.M. Butler,⁶⁰ J. Bystricky,¹⁸ S. Caron,³³ W. Carvalho,³ B.C.K. Casey,⁷³ N.M. Cason,⁵⁴ H. Castilla-Valdez,³² S. Chakrabarti,²⁹ D. Chakraborty,⁵¹ K.M. Chan,⁶⁸ A. Chandra,²⁹ D. Chapin,⁷³ F. Charles,¹⁹ E. Cheu,⁴⁴ D.K. Cho,⁶⁸ S. Choi,⁴⁷ B. Choudhary,²⁸ T. Christiansen,²⁵ L. Christofek,⁵⁶ D. Claes,⁶⁵ B. Clément,¹⁹ C. Clément,⁴⁰ Y. Coadou,⁵ M. Cooke,⁷⁶ W.E. Cooper,⁴⁹ D. Coppage,⁵⁶ M. Corcoran,⁷⁶ A. Cothenet,¹⁵ M.-C. Cousinou,¹⁵ B. Cox,⁴³ S. Crépé-Renaudin,¹⁴ M. Cristetiu,⁴⁷ D. Cutts,⁷³ H. da Motta,² B. Davies,⁴¹ G. Davies,⁴² G.A. Davis,⁵² K. De,⁷⁴ P. de Jong,³³ S.J. de Jong,³⁴ E. De La Cruz-Burelo,³² C. De Oliveira Martins,³ S. Dean,⁴³ J.D. Degenhardt,⁶² F. Déliot,¹⁸ M. Demarteau,⁴⁹ R. Demina,⁶⁸ P. Demine,¹⁸ D. Denisov,⁴⁹ S.P. Denisov,³⁸ S. Desai,⁶⁹ H.T. Diehl,⁴⁹ M. Diesburg,⁴⁹ M. Doidge,⁴¹ H. Dong,⁶⁹ S. Doulas,⁶¹ L.V. Dudko,³⁷ L. Duflot,¹⁶ S.R. Dugad,²⁹ A. Duperrin,¹⁵ J. Dyer,⁶³ A. Dyshkant,⁵¹ M. Eads,⁵¹ D. Edmunds,⁶³ T. Edwards,⁴³ J. Ellison,⁴⁷ J. Elmsheuser,²⁵ V.D. Elvira,⁴⁹ S. Eno,⁵⁹ P. Ermolov,³⁷ O.V. Eroshin,³⁸ J. Estrada,⁴⁹ D. Evans,⁴² H. Evans,⁶⁷ A. Evdokimov,³⁶ V.N. Evdokimov,³⁸ J. Fast,⁴⁹ S.N. Fataki,⁶⁰ L. Feligioni,⁶⁰ T. Ferbel,⁶⁸ F. Fiedler,²⁵ F. Filthaut,³⁴ W. Fisher,⁶⁶ H.E. Fisk,⁴⁹ I. Fleck,²³ M. Fortner,⁵¹ H. Fox,²³ S. Fu,⁴⁹ S. Fuess,⁴⁹ T. Gadfort,⁷⁸ C.F. Galea,³⁴ E. Gallas,⁴⁹ E. Galyaev,⁵⁴ C. Garcia,⁶⁸ A. Garcia-Bellido,⁷⁸ J. Gardner,⁵⁶ V. Gavrilov,³⁶ P. Gay,¹³ D. Gelé,¹⁹ R. Gelhaus,⁴⁷ K. Genser,⁴⁹ C.E. Gerber,⁵⁰ Y. Gershtein,⁴⁸ G. Ginther,⁶⁸ T. Golling,²² B. Gómez,⁸ K. Gounder,⁴⁹ A. Goussiou,⁵⁴ P.D. Grannis,⁶⁹ S. Greder,³ H. Greenlee,⁴⁹ Z.D. Greenwood,⁵⁸ E.M. Gregores,⁴ Ph. Gris,¹³ J.-F. Grivaz,¹⁶ L. Groer,⁶⁷ S. Grünendahl,⁴⁹ M.W. Grünewald,³⁰ S.N. Gurzhiev,³⁸ G. Gutierrez,⁴⁹ P. Gutierrez,⁷² A. Haas,⁶⁷ N.J. Hadley,⁵⁹ S. Hagopian,⁴⁸ I. Hall,⁷² R.E. Hall,⁴⁶ C. Han,⁶² L. Han,⁷ K. Hanagaki,⁴⁹ K. Harder,⁵⁷ R. Harrington,⁶¹ J.M. Hauptman,⁵⁵ R. Hauser,⁶³ J. Hays,⁵² T. Hebbeker,²¹ D. Hedin,⁵¹ J.M. Heinmiller,⁵⁰ A.P. Heinson,⁴⁷ U. Heintz,⁶⁰ C. Hensel,⁵⁶ G. Hesketh,⁶¹ M.D. Hildreth,⁵⁴ R. Hirosky,⁷⁷ J.D. Hobbs,⁶⁹ B. Hoeneisen,¹² M. Hohlfeld,²⁴ S.J. Hong,³¹ R. Hooper,⁷³ P. Houben,³³ Y. Hu,⁶⁹ J. Huang,⁵³ I. Iashvili,⁴⁷ R. Illingworth,⁴⁹ A.S. Ito,⁴⁹ S. Jabeen,⁵⁶ M. Jaffré,¹⁶ S. Jain,⁷² V. Jain,⁷⁰ K. Jakobs,²³ A. Jenkins,⁴² R. Jesik,⁴² K. Johns,⁴⁴ M. Johnson,⁴⁹ A. Jonckheere,⁴⁹ P. Jonsson,⁴² A. Juste,⁴⁹ D. Käfer,²¹ W. Kahl,⁵⁷ S. Kahn,⁷⁰ E. Kajfasz,¹⁵ A.M. Kalinin,³⁵ J. Kalk,⁶³ D. Karmanov,³⁷ J. Kasper,⁶⁰ D. Kau,⁴⁸ R. Kaur,²⁷ R. Kehoe,⁷⁵ S. Kermiche,¹⁵ S. Kesisoglou,⁷³ A. Khanov,⁶⁸ A. Kharchilava,⁵⁴ Y.M. Kharzeev,³⁵ H. Kim,⁷⁴ B. Klima,⁴⁹ M. Klute,²² J.M. Kohli,²⁷ M. Kopal,⁷² V.M. Korablev,³⁸ J. Kotcher,⁷⁰ B. Kothari,⁶⁷ A. Koubarovsky,³⁷ A.V. Kozelov,³⁸ J. Kozminski,⁶³ A. Kryemadhi,⁷⁷ S. Krzywdzinski,⁴⁹ S. Kuleshov,³⁶ Y. Kulik,⁴⁹ A. Kumar,²⁸ S. Kunori,⁵⁹ A. Kupco,¹¹ T. Kurča,²⁰ J. Kvita,¹¹ S. Lager,⁴⁰ N. Lahrichi,¹⁸ G. Landsberg,⁷³ J. Lazoflores,⁴⁸ A.-C. Le Bihan,¹⁹ P. Lebrun,²⁰ W.M. Lee,⁴⁸ A. Leflat,³⁷ F. Lehner,^{49,*} C. Leonidopoulos,⁶⁷ J. Leveque,⁴⁴ P. Lewis,⁴² J. Li,⁷⁴ Q.Z. Li,⁴⁹ J.G.R. Lima,⁵¹ D. Lincoln,⁴⁹ S.L. Linn,⁴⁸ J. Linnemann,⁶³ V.V. Lipaev,³⁸ R. Lipton,⁴⁹ L. Lobo,⁴² A. Lobodenko,³⁹ M. Lokajicek,¹¹ A. Lounis,¹⁹ P. Love,⁴¹ H.J. Lubatti,⁷⁸ L. Lueking,⁴⁹ M. Lynker,⁵⁴ A.L. Lyon,⁴⁹ A.K.A. Maciel,⁵¹ R.J. Madaras,⁴⁵ P. Mättig,²⁶ C. Magass,²¹ A. Magerkurth,⁶² A.-M. Magnan,¹⁴ N. Makovec,¹⁶ P.K. Mal,²⁹ H.B. Malbouisson,³ S. Malik,⁵⁸ V.L. Malyshev,³⁵ H.S. Mao,⁶ Y. Maravin,⁴⁹ M. Martens,⁴⁹ S.E.K. Mattingly,⁷³ A.A. Mayorov,³⁸ R. McCarthy,⁶⁹ R. McCroskey,⁴⁴ D. Meder,²⁴ H.L. Melanson,⁴⁹ A. Melnitchouk,⁶⁴ A. Mendes,¹⁵ M. Merkin,³⁷ K.W. Merritt,⁴⁹ A. Meyer,²¹ M. Michaut,¹⁸ H. Miettinen,⁷⁶ J. Mitrevski,⁶⁷ N. Mokhov,⁴⁹ J. Molina,³ N.K. Mondal,²⁹ R.W. Moore,⁵ G.S. Muanza,²⁰ M. Mulders,⁴⁹ Y.D. Mutaf,⁶⁹ E. Nagy,¹⁵ M. Narain,⁶⁰ N.A. Naumann,³⁴ H.A. Neal,⁶² J.P. Negret,⁸ S. Nelson,⁴⁸ P. Neustroev,³⁹ C. Noeding,²³ A. Nomerotski,⁴⁹ S.F. Novaes,⁴ T. Nunnemann,²⁵ E. Nurse,⁴³ V. O'Dell,⁴⁹ D.C. O'Neil,⁵ V. Oguri,³

N. Oliveira,³ N. Oshima,⁴⁹ G.J. Otero y Garzón,⁵⁰ P. Padley,⁷⁶ N. Parashar,⁵⁸ S.K. Park,³¹ J. Parsons,⁶⁷ R. Partridge,⁷³ N. Parua,⁶⁹ A. Patwa,⁷⁰ P.M. Perea,⁴⁷ E. Perez,¹⁸ P. Pétroff,¹⁶ M. Petteni,⁴² L. Phaf,³³ R. Piegaia,¹ M.-A. Pleier,⁶⁸ P.L.M. Podesta-Lerma,³² V.M. Podstavkov,⁴⁹ Y. Pogorelov,⁵⁴ B.G. Pope,⁶³ W.L. Prado da Silva,³ H.B. Prosper,⁴⁸ S. Protopopescu,⁷⁰ J. Qian,⁶² A. Quadt,²² B. Quinn,⁶⁴ K.J. Rani,²⁹ K. Ranjan,²⁸ P.A. Rapidis,⁴⁹ P.N. Ratoff,⁴¹ N.W. Reay,⁵⁷ S. Reucroft,⁶¹ M. Rijssenbeek,⁶⁹ I. Ripp-Baudot,¹⁹ F. Rizatdinova,⁵⁷ R.F. Rodrigues,³ C. Royon,¹⁸ P. Rubinov,⁴⁹ R. Ruchti,⁵⁴ V.I. Rud,³⁷ G. Sajot,¹⁴ A. Sánchez-Hernández,³² M.P. Sanders,⁵⁹ A. Santoro,³ G. Savage,⁴⁹ L. Sawyer,⁵⁸ T. Scanlon,⁴² D. Schaile,²⁵ R.D. Schamberger,⁶⁹ H. Schellman,⁵² P. Schieferdecker,²⁵ C. Schmitt,²⁶ A. Schwartzman,⁶⁶ R. Schwienhorst,⁶³ S. Sengupta,⁴⁸ H. Severini,⁷² E. Shabalina,⁵⁰ M. Shamim,⁵⁷ V. Shary,¹⁸ A.A. Shchukin,³⁸ W.D. Shephard,⁵⁴ R.K. Shivpuri,²⁸ D. Shpakov,⁶¹ R.A. Sidwell,⁵⁷ V. Simak,¹⁰ V. Sirotenko,⁴⁹ P. Skubic,⁷² P. Slattery,⁶⁸ R.P. Smith,⁴⁹ K. Smolek,¹⁰ G.R. Snow,⁶⁵ J. Snow,⁷¹ S. Snyder,⁷⁰ S. Söldner-Rembold,⁴³ X. Song,⁵¹ L. Sonnenschein,¹⁷ A. Sopczak,⁴¹ M. Sosebee,⁷⁴ K. Soustruznik,⁹ M. Souza,² B. Spurlock,⁷⁴ N.R. Stanton,⁵⁷ J. Stark,¹⁴ J. Steele,⁵⁸ K. Stevenson,⁵³ V. Stolin,³⁶ A. Stone,⁵⁰ D.A. Stoyanova,³⁸ J. Strandberg,⁴⁰ M.A. Strang,⁷⁴ M. Strauss,⁷² R. Ströhmer,²⁵ D. Strom,⁵² M. Strovink,⁴⁵ L. Stutte,⁴⁹ S. Sumowidagdo,⁴⁸ A. Szajdor,³ M. Talby,¹⁵ P. Tamburello,⁴⁴ W. Taylor,⁵ P. Telford,⁴³ J. Temple,⁴⁴ E. Thomas,¹⁵ B. Thooris,¹⁸ M. Tomoto,⁴⁹ T. Toole,⁵⁹ J. Torborg,⁵⁴ S. Towers,⁶⁹ T. Trefzger,²⁴ S. Trincaz-Duvold,¹⁷ B. Tuchming,¹⁸ C. Tully,⁶⁶ A.S. Turcot,⁷⁰ P.M. Tuts,⁶⁷ L. Uvarov,³⁹ S. Uvarov,³⁹ S. Uzunyan,⁵¹ B. Vachon,⁵ R. Van Kooten,⁵³ W.M. van Leeuwen,³³ N. Varelas,⁵⁰ E.W. Varnes,⁴⁴ A. Vartapetian,⁷⁴ I.A. Vasilyev,³⁸ M. Vaupel,²⁶ P. Verdier,¹⁶ L.S. Vertogradov,³⁵ M. Verzocchi,⁵⁹ F. Villeneuve-Seguier,⁴² J.-R. Vlimant,¹⁷ E. Von Toerne,⁵⁷ M. Vreeswijk,³³ T. Vu Anh,¹⁶ H.D. Wahl,⁴⁸ R. Walker,⁴² L. Wang,⁵⁹ Z.-M. Wang,⁶⁹ J. Warchol,⁵⁴ G. Watts,⁷⁸ M. Wayne,⁵⁴ M. Weber,⁴⁹ H. Weerts,⁶³ M. Wegner,²¹ N. Wermes,²² A. White,⁷⁴ V. White,⁴⁹ D. Wicke,⁴⁹ D.A. Wijngaarden,³⁴ G.W. Wilson,⁵⁶ S.J. Wimpenny,⁴⁷ J. Wittlin,⁶⁰ M. Wobisch,⁴⁹ J. Womersley,⁴⁹ D.R. Wood,⁶¹ T.R. Wyatt,⁴³ Q. Xu,⁶² N. Xuan,⁵⁴ S. Yacoob,⁵² R. Yamada,⁴⁹ M. Yan,⁵⁹ T. Yasuda,⁴⁹ Y.A. Yatsunenko,³⁵ Y. Yen,²⁶ K. Yip,⁷⁰ H.D. Yoo,⁷³ S.W. Youn,⁵² J. Yu,⁷⁴ A. Yurkewicz,⁶⁹ A. Zabi,¹⁶ A. Zatserklyaniy,⁵¹ M. Zdrrazil,⁶⁹ C. Zeitnitz,²⁴ D. Zhang,⁴⁹ X. Zhang,⁷² T. Zhao,⁷⁸ Z. Zhao,⁶² B. Zhou,⁶² J. Zhu,⁶⁹ M. Zielinski,⁶⁸ D. Ziemińska,⁵³ A. Ziemiński,⁵³ R. Zitoun,⁶⁹ V. Zutshi,⁵¹ and E.G. Zverev³⁷ (DØ Collaboration)

¹ Universidad de Buenos Aires, Buenos Aires, Argentina

² LAFEX, Centro Brasileiro de Pesquisas Físicas, Rio de Janeiro, Brazil

³ Universidade do Estado do Rio de Janeiro, Rio de Janeiro, Brazil

⁴ Instituto de Física Teórica, Universidade Estadual Paulista, São Paulo, Brazil

⁵ University of Alberta, Edmonton, Alberta, Canada, Simon Fraser University, Burnaby, British Columbia, Canada, York University, Toronto, Ontario, Canada, and McGill University, Montreal, Quebec, Canada

⁶ Institute of High Energy Physics, Beijing, People's Republic of China

⁷ University of Science and Technology of China, Hefei, People's Republic of China

⁸ Universidad de los Andes, Bogotá, Colombia

⁹ Center for Particle Physics, Charles University, Prague, Czech Republic

¹⁰ Czech Technical University, Prague, Czech Republic

¹¹ Institute of Physics, Academy of Sciences, Center for Particle Physics, Prague, Czech Republic

¹² Universidad San Francisco de Quito, Quito, Ecuador

¹³ Laboratoire de Physique Corpusculaire, IN2P3-CNRS, Université Blaise Pascal, Clermont-Ferrand, France

¹⁴ Laboratoire de Physique Subatomique et de Cosmologie, IN2P3-CNRS, Université de Grenoble 1, Grenoble, France

¹⁵ CPPM, IN2P3-CNRS, Université de la Méditerranée, Marseille, France

¹⁶ Laboratoire de l'Accélérateur Linéaire, IN2P3-CNRS, Orsay, France

¹⁷ LPNHE, IN2P3-CNRS, Universités Paris VI and VII, Paris, France

¹⁸ DAPNIA/Service de Physique des Particules, CEA, Saclay, France

¹⁹ IReS, IN2P3-CNRS, Université Louis Pasteur, Strasbourg, France, and Université de Haute Alsace, Mulhouse, France

²⁰ Institut de Physique Nucléaire de Lyon, IN2P3-CNRS, Université Claude Bernard, Villeurbanne, France

²¹ III. Physikalisches Institut A, RWTH Aachen, Aachen, Germany

²² Physikalisches Institut, Universität Bonn, Bonn, Germany

²³ Physikalisches Institut, Universität Freiburg, Freiburg, Germany

²⁴ Institut für Physik, Universität Mainz, Mainz, Germany

²⁵ Ludwig-Maximilians-Universität München, München, Germany

²⁶ Fachbereich Physik, University of Wuppertal, Wuppertal, Germany

²⁷ Panjab University, Chandigarh, India

²⁸ Delhi University, Delhi, India

²⁹ Tata Institute of Fundamental Research, Mumbai, India

³⁰ University College Dublin, Dublin, Ireland

³¹ Korea Detector Laboratory, Korea University, Seoul, Korea

- ³²*CINVESTAV, Mexico City, Mexico*
³³*FOM-Institute NIKHEF and University of Amsterdam/NIKHEF, Amsterdam, The Netherlands*
³⁴*Radboud University Nijmegen/NIKHEF, Nijmegen, The Netherlands*
³⁵*Joint Institute for Nuclear Research, Dubna, Russia*
³⁶*Institute for Theoretical and Experimental Physics, Moscow, Russia*
³⁷*Moscow State University, Moscow, Russia*
³⁸*Institute for High Energy Physics, Protvino, Russia*
³⁹*Petersburg Nuclear Physics Institute, St. Petersburg, Russia*
⁴⁰*Lund University, Lund, Sweden, Royal Institute of Technology and Stockholm University, Stockholm, Sweden, and Uppsala University, Uppsala, Sweden*
⁴¹*Lancaster University, Lancaster, United Kingdom*
⁴²*Imperial College, London, United Kingdom*
⁴³*University of Manchester, Manchester, United Kingdom*
⁴⁴*University of Arizona, Tucson, Arizona 85721, USA*
⁴⁵*Lawrence Berkeley National Laboratory and University of California, Berkeley, California 94720, USA*
⁴⁶*California State University, Fresno, California 93740, USA*
⁴⁷*University of California, Riverside, California 92521, USA*
⁴⁸*Florida State University, Tallahassee, Florida 32306, USA*
⁴⁹*Fermi National Accelerator Laboratory, Batavia, Illinois 60510, USA*
⁵⁰*University of Illinois at Chicago, Chicago, Illinois 60607, USA*
⁵¹*Northern Illinois University, DeKalb, Illinois 60115, USA*
⁵²*Northwestern University, Evanston, Illinois 60208, USA*
⁵³*Indiana University, Bloomington, Indiana 47405, USA*
⁵⁴*University of Notre Dame, Notre Dame, Indiana 46556, USA*
⁵⁵*Iowa State University, Ames, Iowa 50011, USA*
⁵⁶*University of Kansas, Lawrence, Kansas 66045, USA*
⁵⁷*Kansas State University, Manhattan, Kansas 66506, USA*
⁵⁸*Louisiana Tech University, Ruston, Louisiana 71272, USA*
⁵⁹*University of Maryland, College Park, Maryland 20742, USA*
⁶⁰*Boston University, Boston, Massachusetts 02215, USA*
⁶¹*Northeastern University, Boston, Massachusetts 02115, USA*
⁶²*University of Michigan, Ann Arbor, Michigan 48109, USA*
⁶³*Michigan State University, East Lansing, Michigan 48824, USA*
⁶⁴*University of Mississippi, University, Mississippi 38677, USA*
⁶⁵*University of Nebraska, Lincoln, Nebraska 68588, USA*
⁶⁶*Princeton University, Princeton, New Jersey 08544, USA*
⁶⁷*Columbia University, New York, New York 10027, USA*
⁶⁸*University of Rochester, Rochester, New York 14627, USA*
⁶⁹*State University of New York, Stony Brook, New York 11794, USA*
⁷⁰*Brookhaven National Laboratory, Upton, New York 11973, USA*
⁷¹*Langston University, Langston, Oklahoma 73050, USA*
⁷²*University of Oklahoma, Norman, Oklahoma 73019, USA*
⁷³*Brown University, Providence, Rhode Island 02912, USA*
⁷⁴*University of Texas, Arlington, Texas 76019, USA*
⁷⁵*Southern Methodist University, Dallas, Texas 75275, USA*
⁷⁶*Rice University, Houston, Texas 77005, USA*
⁷⁷*University of Virginia, Charlottesville, Virginia 22901, USA*
⁷⁸*University of Washington, Seattle, Washington 98195, USA*

(Dated: March 8, 2005)

We present measurements of the inclusive production cross sections of the $\Upsilon(1S)$ bottomonium state in $p\bar{p}$ collisions at $\sqrt{s} = 1.96$ TeV. Using the $\Upsilon(1S) \rightarrow \mu^+\mu^-$ decay mode for a data sample of $159 \pm 10 \text{ pb}^{-1}$ collected by the DØ detector at the Fermilab Tevatron collider, we determine the differential cross sections as a function of the $\Upsilon(1S)$ transverse momentum for three ranges of the $\Upsilon(1S)$ rapidity: $0 < |y^\Upsilon| \leq 0.6$, $0.6 < |y^\Upsilon| \leq 1.2$, and $1.2 < |y^\Upsilon| \leq 1.8$.

PACS numbers: 13.85.Qk

Quarkonium production in hadron-hadron collisions provides insight into the nature of strong interactions. It is a window on the boundary region between perturbative and non-perturbative QCD. Recent advances in the

understanding of quarkonium production have been stimulated by the unexpectedly large cross sections for direct J/ψ and $\psi(2S)$ production at large transverse momentum (p_T) measured at the Fermilab Tevatron collider [1].

Bottomonium states are produced either promptly or indirectly as a result of the decay of a higher mass state [2], e.g. in a radiative decay such as $\chi_b \rightarrow \Upsilon(1S)\gamma$. The only detailed studies of $\Upsilon(nS)$ production at the Tevatron have been done by the CDF Collaboration [2, 3] in the limited Υ rapidity range of $|y^\Upsilon| < 0.4$ at $\sqrt{s} = 1.8$ TeV, where $y = \frac{1}{2} \ln \frac{E+p_z}{E-p_z}$, E is the Υ energy, and p_z is the Υ momentum parallel to the beam direction.

Three types of models have been used to describe prompt quarkonium formation: the color-singlet model [4], the color-evaporation model [5] (and a follow-up soft color interaction model [6]), and the color-octet model [7]. These models of quarkonium formation lead to different expectations for the production rates and polarization of the quarkonium states, yet many of the model parameters have to be extracted directly from the data. A recent paper [8, 9] successfully reproduces the shape of the p_T distribution of Υ states produced at Tevatron energies by combining separate perturbative approaches for the low- and high- p_T regions. The absolute cross section is not predicted by these calculations, which are similar to the color-evaporation model.

In this Letter we concentrate on the production of the $\Upsilon(1S)$ state. A precise measurement of the differential $\Upsilon(1S)$ cross section, using the wide rapidity range accessible by the DØ detector, will provide valuable input to the various quarkonium production models. By reconstructing the $\Upsilon(1S)$ through its decay $\Upsilon(1S) \rightarrow \mu^+ \mu^-$, we determine production cross sections of the $\Upsilon(1S)$ as a function of its transverse momentum, in three rapidity ranges: $0 < |y^\Upsilon| \leq 0.6$, $0.6 < |y^\Upsilon| \leq 1.2$, and $1.2 < |y^\Upsilon| \leq 1.8$.

The DØ detector is described in detail elsewhere [10]. Here, we briefly describe only the detector components most relevant to this analysis. The DØ tracking system consists of a high-resolution silicon microstrip tracker (SMT) surrounded by a central scintillating-fiber tracker (CFT) inside a 2 T magnetic field provided by a superconducting solenoid. The tracking volume extends to a radius of approximately 52 cm. Closest to the interaction region is the SMT with a typical strip pitch of 50–80 μm . It has a barrel-disk hybrid structure and provides tracking and vertexing coverage in the pseudorapidity range $|\eta| < 3.0$, where $\eta = -\ln[\tan(\theta/2)]$ and θ is the polar angle. The CFT consists of eight concentric cylinders of pairs of scintillating-fiber doublets. On each cylinder, the inner doublet runs parallel to the beam axis and the outer doublet is mounted at a stereo angle of $\pm 3^\circ$, alternating with each cylinder. Located outside the superconducting coil is the uranium-liquid-argon calorimeter. Beyond the calorimeter, the muon system consists of three layers of drift tubes, 10 cm wide in the central region ($|\eta| < 1$) and 1 cm in the forward region ($1 < |\eta| < 2$). Interspersed between the drift tubes are scintillating counters. Located between the innermost and the middle layers of drift tubes are 1.8 T iron toroid magnets. DØ uses up to

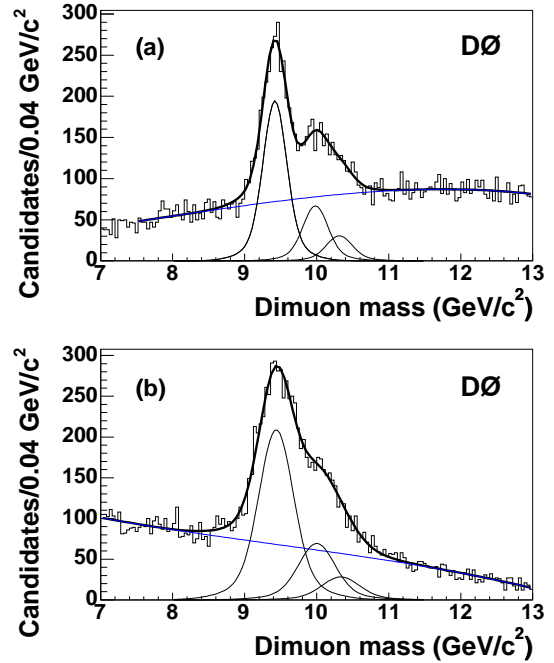


FIG. 1: Example of fits to the dimuon spectra in different bins of rapidity in the p_T bin of $4 \text{ GeV}/c < p_T^\Upsilon < 6 \text{ GeV}/c$: (a) $|y^\Upsilon| \leq 0.6$, (b) $1.2 < |y^\Upsilon| \leq 1.8$. The heavy line shows the combined fit for signal and background. Also shown are the individual contributions from the three Υ states and the background separately.

three levels of triggers to reduce the initial event rate of 1.7 MHz to an output rate of approximately 50 Hz.

The data were collected between June 2002 and September 2003 and correspond to an integrated luminosity of $159 \pm 10 \text{ pb}^{-1}$ for the chosen two triggers. These triggers are scintillator-based dimuon triggers at the first trigger level and require the confirmation of one or both muons at the second trigger level. The first trigger level is almost fully efficient for muons with a transverse momentum above $5 \text{ GeV}/c$. For events passing our analysis criteria, the second level trigger requirement kept more than 97% of events which satisfied the first level requirement.

The analysis requires two oppositely charged muons with $p_T^\mu > 3 \text{ GeV}/c$ and $|y^\mu| < 2.2$. Only muons that are matched to a track found by the central tracking system and which have hits inside and outside the toroidal magnets are used. The track associated with a muon must have at least one hit in the SMT. We reject cosmic ray muons based on timing information from the muon system scintillators. Compared to muons from the dominant $b\bar{b}$ background, muons from $\Upsilon(nS)$ decays are expected to be relatively isolated, and therefore we require at least one of the muons to satisfy the following criterion: either the sum of the transverse momenta of charged tracks in

a cone of radius 0.5 (in η - ϕ space) around the muon is less than 1 GeV or the sum of the calorimeter transverse energies in an annular cone of radii 0.1 and 0.5 around the muon is less than 1 GeV. This isolation requirement reduces the background by 35% and the signal by less than 6%.

Two typical examples of dimuon mass distributions in different rapidity bins are shown in Fig. 1. In each plot a strong $\Upsilon(1S)$ signal can be seen, accompanied by a shoulder attributed to unresolved signals due to $\Upsilon(2S)$ and $\Upsilon(3S)$ production. The mass distributions are fit starting from 7.0, 7.5 or 7.8 GeV/c^2 , depending on p_T^Υ and y^Υ , to 13.0 GeV/c^2 using separate mass resolution functions for each of the $\Upsilon(nS)$ states and a third-order polynomial for the background. The mass resolution function is approximated by a sum of two Gaussians with the relative contribution and width of the second Gaussian fixed

with respect to the first Gaussian. The values of this contribution were determined from Monte Carlo studies and J/ψ signal fits to data. The mass of the $\Upsilon(1S)$ is a free parameter of the fit and the remaining two masses are shifted by the $m(\Upsilon(nS)) - m(\Upsilon(1S))$ differences of 563 MeV/c^2 ($\Upsilon(2S)$) and 895 MeV/c^2 ($\Upsilon(3S)$), taken from Ref. [11]. In addition, only the width of the $\Upsilon(1S)$ state is allowed to vary. The widths of the other states are assumed to scale with the mass of the resonance. Normalizations of functions representing each resonance are free parameters of the fit. The Monte Carlo samples used in this study were generated with PYTHIA v6.202 [12]. The muon kinematic distributions from data and Monte Carlo agree within a given p_T^Υ and y^Υ bin.

The cross section for a given kinematic range, multiplied by the branching fraction $\Upsilon(1S) \rightarrow \mu^+ \mu^-$, is given by:

$$\frac{d^2\sigma(\Upsilon(1S))}{dp_T \cdot dy} \times \mathcal{B}(\Upsilon(1S) \rightarrow \mu^+ \mu^-) = \frac{N(\Upsilon(1S))}{\mathcal{L} \cdot \Delta p_T \cdot \Delta y \cdot \varepsilon_{acc} \cdot \varepsilon_{trig} \cdot k_{qual} \cdot k_{trk} \cdot k_{dimu}}, \quad (1)$$

where \mathcal{L} is the integrated luminosity for the data sample used, $N(\Upsilon(1S))$ is the number of observed $\Upsilon(1S)$, and the ε and k represent the various efficiency, acceptance and correction factors. The $\Upsilon(1S)$ acceptance and reconstruction efficiency ε_{acc} represents the fraction of generated $\Upsilon(1S)$ events that are successfully reconstructed in the DØ detector, not taking into account any loss in efficiency due to triggering. Its value is based on a Monte Carlo analysis. The dimuon trigger efficiency ε_{trig} for reconstructed $\Upsilon(1S)$ events that satisfy our analysis criteria is estimated using a trigger simulation and verified directly with the data using other triggers. The remaining factors in Eq. 1 account for the differences between the data and Monte Carlo and are referred to as corrections, rather than efficiencies. The correction k_{qual} takes into account differences in the track quality requirements, i.e. the isolation and SMT hit requirements and cosmic ray rejection. It is consistent with being independent of p_T and its value varies between 0.85 and 0.93 with increasing rapidity. The central tracking correction k_{trk} takes into account both differences in the tracking and the track-to-muon matching efficiency. It is derived from the J/ψ data sample and Monte Carlo simulation and is very close to unity except for the forward rapidity region where $k_{trk} \approx 0.95$. The correction factor k_{dimu} accounts for the differences in the local (i.e. muon system only) muon reconstruction, taking into account trigger effects. It was determined using J/ψ candidates collected with single muon triggers. It does not show a significant p_T dependence, but it changes with the muon rapidity.

In Table I we summarize the values of efficiencies found in different rapidity regions. The measured cross sections are collected in Table II. These cross sections are normalized per unit of rapidity.

TABLE I: Efficiencies used in the cross section calculations.

$ y^\Upsilon $	ε_{acc}	ε_{trig}	k_{qual}	k_{trk}	k_{dimu}
0.0 – 0.6	0.15 – 0.26	0.70	0.85	0.99	0.85
0.6 – 1.2	0.19 – 0.28	0.73	0.85	0.99	0.88
1.2 – 1.8	0.20 – 0.27	0.82	0.93	0.95	0.95

Differential cross sections, normalized to unity, are summarized in Table III. Figure 2 shows these cross sections compared to theoretical predictions from Ref. [9]. There is little variation in the shape of the p_T distributions with rapidity. This is further illustrated in Fig. 3 which shows the ratio of the differential cross sections of $\sigma(1.2 < |y^\Upsilon| \leq 1.8)$ to $\sigma(|y^\Upsilon| \leq 0.6)$. In Fig. 4 we show a comparison with results from CDF [3].

The overall systematic uncertainties, excluding luminosity, are approximately 10%. The uncertainty on the luminosity [13] is 6.5%. The main systematic errors are due to the fitting procedure and the determination of k_{dimu} . The statistical uncertainty of the fitted number of events in a given kinematic bin and the uncertainty from varying the contribution of the second Gaussian are added in quadrature to give the uncertainties labeled ‘stat’ in Table II. The net effect is an increase in the overall fit uncertainty by less than 40% of its statistical

TABLE II: Fitted number of events and $d\sigma(\Upsilon(1S))/dy \times \mathcal{B}(\Upsilon(1S) \rightarrow \mu^+\mu^-)$ per unit of rapidity.

$ y^\Upsilon $	Number of $\Upsilon(1S)$	$d\sigma(\Upsilon(1S))/dy \times \mathcal{B}(\Upsilon(1S) \rightarrow \mu^+\mu^-)$ (pb)
0.0 – 0.6	$12,951 \pm 336$	732 ± 19 (stat) ± 73 (syst) ± 48 (lum)
0.6 – 1.2	$16,682 \pm 438$	762 ± 20 (stat) ± 76 (syst) ± 50 (lum)
1.2 – 1.8	$17,884 \pm 566$	600 ± 19 (stat) ± 56 (syst) ± 39 (lum)
0.0 – 1.8	$46,625 \pm 939$	695 ± 14 (stat) ± 68 (syst) ± 45 (lum)

TABLE III: Normalized differential cross sections for $\Upsilon(1S)$ in different rapidity regions. Quoted uncertainties include statistical uncertainties added in quadrature to systematic uncertainties due to the assumed shape of the mass resolution function (cf. ‘stat’ uncertainties in Table II). The remaining systematic uncertainties are p_T independent and quoted in Table II.

p_T^Υ (GeV/c)	$0.0 < y^\Upsilon \leq 0.6$	$0.6 < y^\Upsilon \leq 1.2$	$1.2 < y^\Upsilon \leq 1.8$	$0.0 < y^\Upsilon \leq 1.8$
0 – 1	0.051 ± 0.005	0.061 ± 0.006	0.050 ± 0.005	0.056 ± 0.004
1 – 2	0.138 ± 0.010	0.137 ± 0.010	0.136 ± 0.011	0.136 ± 0.008
2 – 3	0.152 ± 0.010	0.153 ± 0.010	0.175 ± 0.015	0.160 ± 0.009
3 – 4	0.149 ± 0.011	0.175 ± 0.012	0.160 ± 0.014	0.159 ± 0.009
4 – 6	0.112 ± 0.006	0.110 ± 0.007	0.115 ± 0.008	0.113 ± 0.005
6 – 8	0.067 ± 0.005	0.061 ± 0.004	0.056 ± 0.005	0.062 ± 0.003
8 – 10	0.034 ± 0.003	0.034 ± 0.003	0.034 ± 0.003	0.035 ± 0.002
10 – 15	0.014 ± 0.001	0.011 ± 0.001	0.011 ± 0.001	0.012 ± 0.001
15 – 20	0.0032 ± 0.0005	0.0019 ± 0.0003	0.0019 ± 0.0004	0.0023 ± 0.0002

uncertainty alone. An additional uncertainty in the fitting procedure due to varying the fitting range and the background parametrization is at the 4% level. The systematic uncertainty for k_{dimu} is 8.7%, 8.2% and 7.2% for the three rapidity bins. These were derived from uncertainties for the Monte Carlo – data differences for individual muons, determined as a function of muon rapidity and transverse momentum. The other uncertainties considered include momentum resolution, uncertainties introduced by the track quality and track matching requirements, variations in the input Monte Carlo distributions, and changes in detector performance over time. All these systematic uncertainties contribute less than 2% each.

The current analysis assumes that the $\Upsilon(1S)$ is produced unpolarized, in agreement with the CDF measurement [3] of the polarization parameter $\alpha = -0.12 \pm 0.22$ for $8 < p_T^\Upsilon < 20$ GeV/c. Although we do not include a contribution to the systematic uncertainty due to this assumption, we estimate the sensitivity of our results to the $\Upsilon(1S)$ polarization by varying α within ± 0.15 (± 0.30). This changes our results by less than 4% (15%) in all p_T bins.

In conclusion, we present a measurement of the inclusive production cross section of the $\Upsilon(1S)$ bottomonium state using the $\Upsilon(1S) \rightarrow \mu^+\mu^-$ decay mode. The measured cross section $\times \mathcal{B}(\Upsilon(1S) \rightarrow \mu^+\mu^-)$ for the $|y^\Upsilon| \leq 0.6$ region is 732 ± 19 (stat) ± 73 (syst) ± 48 (lum) pb. Taking into account a predicted increase in the cross section when the $p\bar{p}$ center-of-mass energy increases from 1.8 TeV to 1.96 TeV [12], our result is compatible with the CDF result [3] of 680 ± 15 (stat) ± 18 (syst) ± 26 (lum)

pb for $\sqrt{s} = 1.8$ TeV. We measure the ratios of the cross sections for the $0.6 < |y^\Upsilon| \leq 1.2$ and $1.2 < |y^\Upsilon| \leq 1.8$ ranges to that for the $|y^\Upsilon| \leq 0.6$ range to be 1.04 ± 0.14 and 0.80 ± 0.11 , compared with predictions from Monte Carlo [12] of 0.94 and 0.83. Between the rapidity regions, there is little variation in the shapes of the differential cross sections, and their shapes agree reasonably well with theoretical predictions [9]. The shape of the combined differential cross section for $|y^\Upsilon| \leq 1.8$ is consistent with the CDF measurement in the limited rapidity range of $|y^\Upsilon| < 0.4$ [3]. The results presented in this Letter will allow a more precise determination of parameters of the various bottomonium production models.

We thank the staffs at Fermilab and collaborating institutions, and acknowledge support from the Department of Energy and National Science Foundation (USA), Commissariat à l’Energie Atomique and CNRS/Institut National de Physique Nucléaire et de Physique des Particules (France), Ministry of Education and Science, Agency for Atomic Energy and RF President Grants Program (Russia), CAPES, CNPq, FAPERJ, FAPESP and FUNDUNESP (Brazil), Departments of Atomic Energy and Science and Technology (India), Colciencias (Colombia), CONACYT (Mexico), KRF (Korea), CONICET and UBACyT (Argentina), The Foundation for Fundamental Research on Matter (The Netherlands), PPARC (United Kingdom), Ministry of Education (Czech Republic), Canada Research Chairs Program, CFI, Natural Sciences and Engineering Research Council and WestGrid Project (Canada), BMBF and DFG (Germany), Science Foundation Ireland, A.P. Sloan Foundation, Research Corporation, Texas Advanced Research Program,

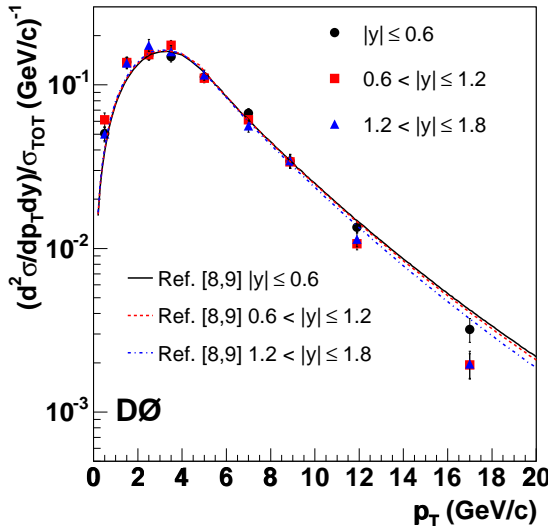


FIG. 2: Normalized differential cross sections for $\Upsilon(1S)$ production compared with theory predictions [8, 9]. The errors shown correspond to the errors in Table III.

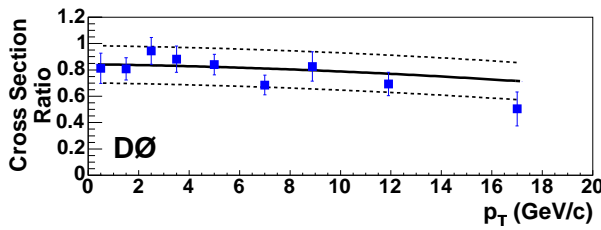


FIG. 3: The ratio of differential cross sections (squares) for $\sigma(1.2 < |y|^{\Upsilon} | \leq 1.8)$ to $\sigma(|y|^{\Upsilon} | \leq 0.6)$. The solid line is the Monte Carlo prediction [12] normalized to the measured ratio of the p_T -integrated cross section. Uncertainties of the relative normalization are indicated by the dashed lines.

Alexander von Humboldt Foundation, and the Marie Curie Fellowships.

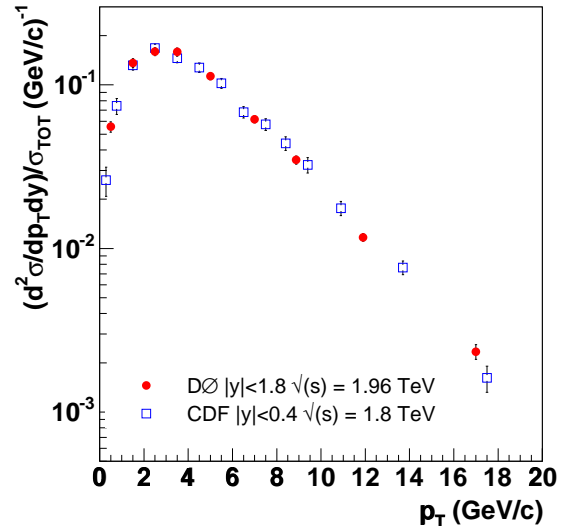


FIG. 4: Normalized differential cross sections for $\Upsilon(1S)$ production at $\sqrt{s} = 1.96$ TeV compared with published CDF results [3] at $\sqrt{s} = 1.8$ TeV. The errors shown are statistical only.

56, 7317 (1997).

- [7] P. Cho and A. Leibovich, Phys. Rev. D **53** 150 (1996); ibid 6203 (1996). E. Braaten, S. Fleming, and A. Leibovich Phys. Rev. D **63** 094006 (2001) and references therein.
- [8] E. L. Berger, J. Qiu, and Y. Wang, Phys Rev D **71** 034007 (2005).
- [9] E. L. Berger, J. Qiu, and Y. Wang, hep-ph/0411026, Nov. 2004.
- [10] DØ Collaboration, V. Abazov *et al.*, in preparation for submission to Nucl. Instrum. Methods Phys. Res. A; T. LeCompte and H.T. Diehl, Ann. Rev. Nucl. Part. Sci. **50**, 71 (2000).
- [11] Particle Data Group, S. Eidelman *et al.*, Phys. Lett. B **592**, 1 (2004).
- [12] T. Sjöstrand, L. Lönnblad, and S. Mrenna, hep-ph/0108264. The PYTHIA quarkonium generator is based on color-singlet calculations by E.W.N. Glover, A.D. Martin, and W.J. Stirling, Z. Phys. C **38**, 473 (1988).
- [13] T. Edwards *et al.*, FERMILAB-TM-2278-E (2004).

[*] Visitor from University of Zurich, Zurich, Switzerland.

- [1] CDF Collaboration, F. Abe *et al.*, Phys. Rev. Lett. **69**, 3704 (1992); ibid, **79**, 572 (1997); ibid, **79**, 578 (1997).
- [2] CDF Collaboration, T. Affolder *et al.*, Phys. Rev. Lett. **84**, 2094 (2000).
- [3] CDF Collaboration, D. Acosta *et al.*, Phys. Rev. Lett. **88**, 161802 (2002).
- [4] R. Baier and R. Rückl, Z. Phys. **C19**, 251 (1983); M. Vanttilinen *et al.*, Phys. Rev. **D51**, 3332 (1995).
- [5] H. Fritzsch, Phys. Lett. **67B**, 217 (1977); C. B. Mariotto, M. B. Ducati, and G. Ingelman, Eur. Phys. J. C **23** 527 (2002), and references therein.
- [6] A. Edin, G. Ingelman, and J. Rathsman, Phys. Rev. D